Origin of the lobe structure in photorefractive beam fanning

G. Montemezzani, A. A. Zozulya, L. Czaia, and D. Z. Anderson
Joint Institute for Laboratory Astrophysics, University of Colorado, Campus Box 440, Boulder, Colorado 80309-0440

M. Zgonik and P. Günter
Nonlinear Optics Laboratory, Institute of Quantum Electronics, Swiss Federal Institute of Technology, CH-8093, Zürich, Switzerland
(Received 10 March 1995)

We show that the three enigmatic lobes or petals observed in the far-field fanning pattern of photorefractive $BaTiO_3$ crystals are correctly predicted by considering the piezoelectric and photoelastic contributions of crystal deformations to the photorefractive nonlinearity.

PACS number(s): 42.65.Hw, 42.40.Pa, 77.65.−j, 78.20.−e

A laser beam passing through a photorefractive medium spreads into a filamenting fan of light that arises from stimulated scattering [1]. This beam fanning is seen on one hand as an impediment to practical applications of photorefractive materials such as holographic storage, yet on the other hand it is the progenitor of such remarkable phenomena as self-pumped and mutual phase conjugation.

Beam fanning is a hallmark of photorefractive nonlinearity whose qualitative physics is well understood: It consists of amplification of low-intensity spatially broadband light scattering by the primary beam as they both propagate through the medium. Roughly speaking, fanning intensity if large in a direction for which two-beam coupling gain between the primary beam and a signal beam traveling in that direction is large. Figure 1 shows an often seen far-field fanning pattern in $BaTiO_3$. The incident laser beam is extraordinarily polarized and propagates along the crystal a or b axis. The fanning is a three-lobed structure consisting of a central lobe in the positive direction of the crystal c axis and two symmetric side lobes or petals making angles of about 55° with the central one. Figure 1 therefore suggests that the gain in the three directions corresponding to the petals is large compared with other directions. Yet the three-lobed pattern is not predicted by textbook formulas [2]: only the central lobe is qualitatively correctly predicted, whereas the flanking petals are not. The standard approaches often fail with other geometries and crystals as well.

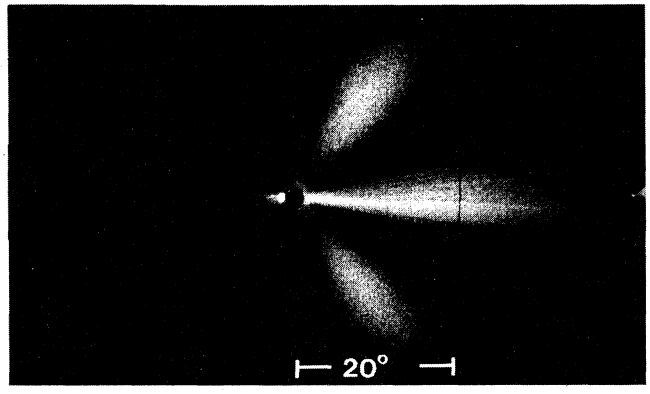

FIG. 1. Far-field intensity distribution of amplified scattered light (fanning) for a pumping beam ($\lambda=514$ nm) propagating through a photorefractive crystal of $BaTiO_3$ along the a axis. Both the pump and the fanning have extraordinary polarization. The crystal c axis points to the right. The pump beam is blocked by the dark spot in the middle; the power going into the petals is about 10% of that of the transmitted pumping beam.

In the standard models of photorefractive interactions, the structure of fanning is primarily buried in the electro-optic tensor and dielectric tensor. Values of these tensors measured under clamped (constant strain) or unclamped (constant stress) conditions are usually used. It has recently been shown that the mechanical consequences of the photorefractive space-charge field can be substantial [3–8]. Fanning structure should therefore also reflect the nature of the elasto-optic and piezoelectric tensors as well as the electro-optic tensor and dielectric tensor.

In this paper, we show that the interplay of electrical, mechanical, and optical effects substantially alters the qualitative nature of beam fanning. In particular, we show that the fanning structures seen in $BaTiO_3$, including the petals shown in Fig. 1, are predicted when mechanical effects are consistently incorporated in the model for two-beam coupling.

We calculate the angular distribution of fanning under the assumption that its level is small. In this case the primary beam is not depleted, and evolution of each plane-wave component of the noise can be studied separately. If the characteristic scattering angles of the noise θ with respect to the primary beam are such that $\theta l < d$, where l is the length of the crystal and d is the beam diameter, the effects of the finite transverse size of the beam are not important, and the beam may be approximated by a plane wave, reducing the problem to that of nonlinear interaction between two plane waves, one of which (signal) is considerably weaker than the other (pump).

A steady-state material response of a photorefractive

medium in the framework of a one-species model (holes), which takes into account induced material deformations, is governed by the set of the following equations [5,9]:

$$(\beta+sI)(N_{A0}-N_A^-)-\xi n_h N_A^-=0 , \tag{1a}$$

$$\vec{\nabla}\cdot\vec{D}=e(n_h-N_A^-+N_{A0}^-) , \tag{1b}$$

$$\vec{\nabla}\cdot(en_h\vec{E}-\kappa_B T\vec{\nabla}n_h)=0 , \tag{1c}$$

$$C_{ijkl}^E\frac{\partial^2 u_k}{\partial x_j\partial x_l}-e_{kij}\frac{\partial E_k}{\partial x_j}=0 , \tag{1d}$$

$$D_i=\epsilon_0\epsilon_{ij}^S E_j+e_{ijk}\frac{\partial u_k}{\partial x_j} , \tag{1e}$$

$$\Delta\left[\frac{1}{n^2}\right]_{ij}=r_{ijk}^S E_k+p_{ijkl}'^E\frac{\partial u_k}{\partial x_l} . \tag{1f}$$

Here N_{A0}, N_A^-, N_{A0}^-, and n_h are the density of acceptors, ionized acceptors, ionized acceptors in the dark, and conducting holes, respectively; β and s are the thermal and photoexcitation coefficients; $I=|\vec{A}|^2$ is the intensity of electromagnetic radiation; ξ is the recombination constant; e is the elementary charge; κ_B is Boltzmann's constant; and T is the temperature. The vectors $\vec{E}$ and $\vec{D}$ are the amplitudes of the static electric field and the electric displacement, respectively; $\vec{u}$ is the displacement vector of the medium; ϵ_0 is the electric permeability of vacuum; ϵ_{ij}^S is the clamped static dielectric tensor; C_{ijkl}^E is the elastic stiffness tensor; and e_{ijk} is the piezoelectric stress tensor. Finally, $\Delta(1/n^2)_{ij}$ is the change in the optical index ellipsoid, r_{ijk}^S is the clamped electro-optic tensor, and $p_{ijkl}'^E$ the elasto-optic tensor at a constant electric field.

If the electromagnetic field $\vec{A}$ in the medium consists of two plane waves

$$\vec{A}=\vec{a}_p A_p\exp(i\vec{k}_p\cdot\vec{r})+\vec{a}_s A_s\exp(i\vec{k}_s\cdot\vec{r}) , \tag{2}$$

and one of them is much stronger than the other $|A_p|^2\gg|A_s|^2$, Eqs. (1) may be linearized and their solution sought in the form

$$I=I^{(0)}+[I^{(1)}\exp(i\vec{K}_g\cdot\vec{r})+\text{c.c.}] , \tag{3a}$$

$$\vec{E}=i\vec{g}\frac{I^{(1)}}{I^{(0)}}E^{(1)}\exp(i\vec{K}_g\cdot\vec{r})+\text{c.c.} , \tag{3b}$$

$$\vec{u}=\frac{E^{(1)}}{K_g}\frac{I^{(1)}}{I^{(0)}}\vec{u}^{(1)}\exp(i\vec{K}_g\cdot\vec{r})+\text{c.c.} , \tag{3c}$$

where $I^{(0)}=|A_p|^2$, $I^{(1)}=A_s A_p^*(\vec{a}_s\cdot\vec{a}_p)$, $\vec{K}_g=\vec{k}_s-\vec{k}_p$, and $\vec{g}=\vec{K}_g/|\vec{K}_g|$. The direction of the static electric field $\vec{E}$ is determined by that of the unit vector of the grating $\vec{g}$ since $\nabla\times\vec{E}\propto\vec{K}_g\times\vec{E}=\vec{0}$.

Under the standard assumptions N_{A0}, $N_{A0}-N_{A0}^-\gg n_h$, and $sI_0\gg\beta$, the solution for the static electric field $E^{(1)}$ can be expressed in the form

$$E^{(1)}=\frac{E_D E_q}{E_D+E_q} , \tag{4}$$

where $E_D=\kappa_B TK_g/e$, $E_q=eN_{\text{eff}}/\epsilon_0\epsilon_{\text{eff}}K_g$, $N_{\text{eff}}=N_{A0}^-(N_{A0}-N_{A0}^-)/N_{A0}$, and the effective static dielectric constant ϵ_{eff} is determined by the relation [5]

$$\epsilon_{\text{eff}}=g_i g_j\left[\epsilon_{ij}^S+\frac{1}{\epsilon_0}e_{ijk}u_k^{(1)}\right] . \tag{5}$$

The function $\vec{u}^{(1)}$ satisfies the equation

$$C_{ijkl}^E g_j g_l u_k^{(1)}-e_{kij}g_j g_k=0 . \tag{6}$$

Its solution can be expressed in the form

$$u_k=A_{ki}^{-1}B_i , \tag{7}$$

where $A_{ik}=C_{ijkl}^E g_j g_l$ and $B_i=e_{kij}g_k g_j$.

The stationary exponential gain coefficient Γ for the propagation of the weak signal wave A_s along its wavevector direction is given by the expression [10]

$$\Gamma=\frac{2\pi}{\lambda}(n_p n_s)^{3/2}r_{\text{eff}}E^{(1)}(\vec{a}_p\cdot\vec{a}_s) , \tag{8}$$

where λ is the wavelength of light in vacuum, n_p and n_s are refractive indices of the pump and the signal waves, respectively, and r_{eff} is the scalar electro-optic coefficient, determined by the relation

$$r_{\text{eff}}=d_{p,i}d_{s,j}[r_{ijk}^S g_k+p_{ijkl}'^E g_l u_k^{(1)}] . \tag{9}$$

Here $\vec{d}_p$ and $\vec{d}_s$ are the unit vectors along the directions of the dielectric displacement vectors (polarization) for the pump and the signal waves, respectively. Note that they are slightly different from the directions of the electric field of the pump and the signal given by the unit vectors $\vec{a}_p$ and $\vec{a}_s$.

Below we present results of calculations for the fanning pattern in the geometry corresponding to Fig 1 and using the recently determined data of Refs. [11,12]. Figure 2 shows a contour map of the gain coefficient Γ as a function of the direction of propagation of the weak signal beam for the effective concentration of traps $N_{\text{eff}}=5\times10^{16}$ cm^{-3}. The e-polarized pump beam is assumed to propagate parallel to the a axis, which corresponds to the center of the plot. The two coordinate axes have been chosen in such a way that each point on the plot corresponds to the point of incidence of a signal ray on a flat screen placed far away behind the crystal, as the one used for the photograph of Fig. 1. The horizontal axis is parallel to the c axis; the vertical axis is parallel to the b axis. Figure 2 spans external angles from $-45°$ to $+45°$ in both directions. The results of Fig 2 are obtained for signal waves with extraordinary polarization. Similar calculations for ordinary polarized signals give much smaller gain coefficients, indicating that in this geometry only extraordinary polarized light gives a significant contribution to the fanning. Figure 2 clearly demonstrates the three-petaled structure of Γ that translates itself into the pattern of Fig. 1. The right part of Fig. 2 (solid contours) corresponds to positive values of the gain coefficient; the fanning waves propagating in these directions are amplified. The left part (dashed contours) has the same structure but with the negative sign; the fanning waves propagating to the left of the pump experience loss. The values of the gain in the central and the side petals and their angular extent are determined by the effective concentration of traps N_{eff}. Larger values of

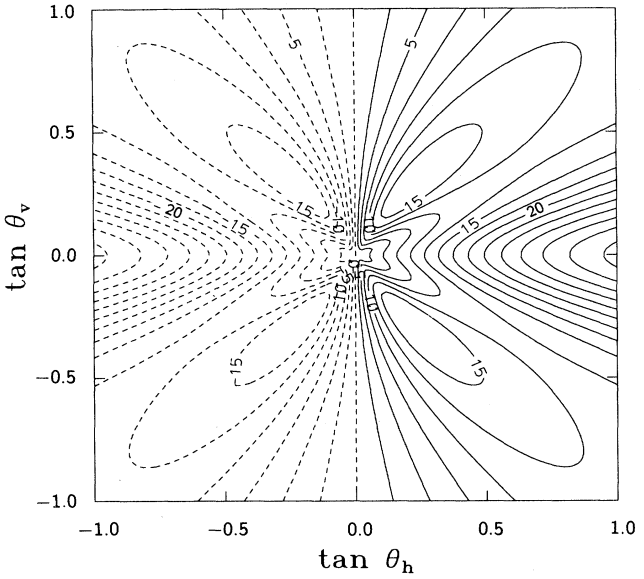

FIG. 2. Contour map of the gain coefficient Γ (in cm^{-1}) in BaT:O_3 for $N_{eff}=5\times10^{16}$ cm^{-3} as obtained by using the equations in the text. The pump propagating along the *a* axis corresponds to the center of the figure; the *c* axis is parallel to the horizontal axis of the figure and points to the right. Both the pump and the signal have extraordinary polarization. Dashed lines correspond to negative values of Γ. The coordinates are the tangents of the horizontal and vertical angles of each signal wave with respect to the pumping wave.

N_{eff} result in the expansion of the petals from the center of Fig. 2; a smaller concentration of traps corresponds to shrinking of the petals towards the center. The maximum value of the gain in the petals also grows with an increase in N_{eff}. Analogous calculations postulating either clamped or unclamped conditions yield very different results. Figure 3 shows the same as Fig. 2 but

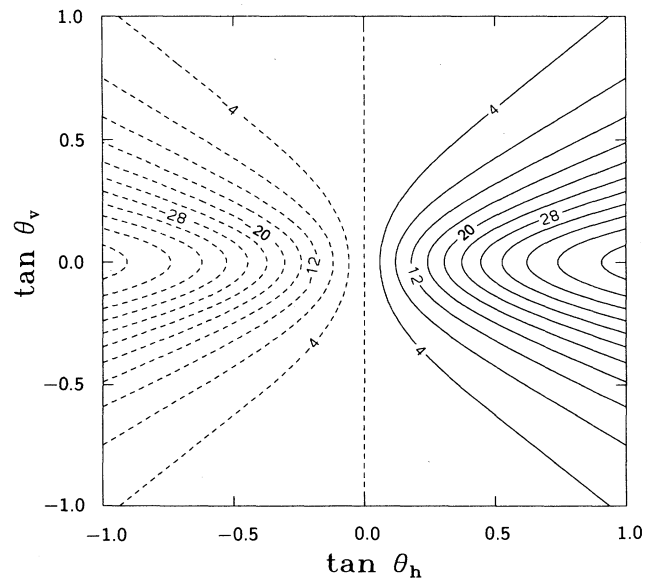

FIG. 3. Same as in Fig. 2 but using unclamped electro-optic coefficients and dielectric constants.

neglects small-scale crystal deformations and uses the unclamped values for the electro-optic constants and the dielectric constant. The gain coefficient has only one petal aligned along the positive direction of the *c* axis. Similar results are obtained by using the clamped coefficients. The absence of the two side petals proves that neither clamped nor unclamped conditions can adequately describe the situation and thereby confirms the validity of the above approach.

Figure 4 shows r_{eff} [Eq. (9)] and ϵ_{eff} [Eq. (5)] for signal waves propagating along a cone with a half angle of 20° with respect to the pumping beam outside the crystal. The abscissa is the azimuthal angle α along a normal section of the cone; only the right side of the cone is plotted. An angle of 0° corresponds to a signal propagating in the *ac* plane, angles of ±90° correspond to signals propagating in the *ab* plane. The solid curves have been obtained in the framework of the above treatment; the dashed curves are for the unclamped situation. The two maxima in r_{eff} at ±60° are responsible for the two side petals of Fig. 1; the maximum at 0° gives rise to the central petal. The experimentally measured angle between the central and side petals along the 20° cone is approximately 55°. This value is slightly less than the angle between the maxima in r_{eff}. The reason is the increase in ϵ_{eff} with the increase in $|\alpha|$ as shown in Fig. 4(b). An increase in ϵ_{eff} reduces the space-charge field through Eq. (4) and thus the amplification gain. For this reason, the maximum gain in Fig. 2 is found on the horizontal axis ($\alpha=0$), even though the effective electro-optic coefficient is larger within the side petals. The inward bending of the contour lines seen in Fig. 2 is also due to the anisotropy of ϵ_{eff}. The effect of ϵ_{eff} on the space-charge field is larger for large grating vectors K_g, that is, for signals propaga-

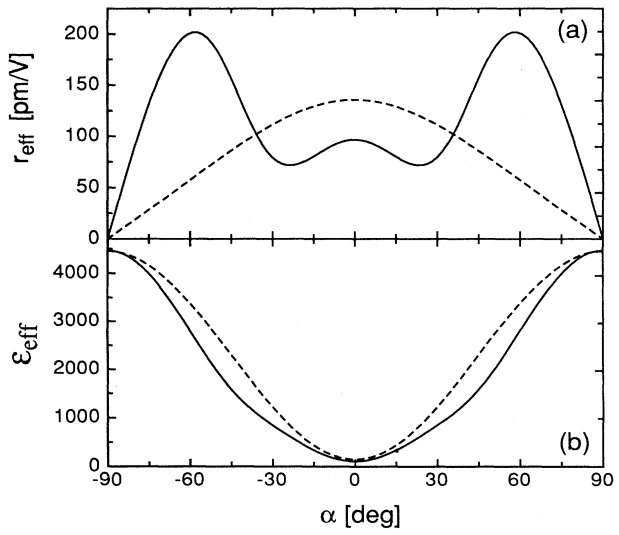

FIG. 4. The effective electro-optic coefficient r_{eff} (a) and dielectric constant ϵ_{eff} (b), for the signal beams propagating at an angle of 20° to the pumping beam outside the crystal. α is the azimuth angle along the cone, with 0° corresponding to a signal in the *ac* plane. Solid curves correspond to the solution of the equations in the text, dashed curves correspond to the unclamped situation.

ting at larger angles with respect to the pump beam.

The output intensity of noise (fanning) I_{out} in any given direction equals its initial intensity I_{in} times the exponential amplification factor $\exp(\Gamma l)$, where $l = L/\cos(\theta)$ is the distance traveled by the noise wave in the crystal, L is the length of the crystal, and θ is the angle between the direction of propagation of the noise wave and the a axis. If the initial noise distribution were uniform in the angular domain, the observed level of fanning would directly reflect the shape of the amplification coefficient Γ. In particular, the maximum fanning intensity would correspond to large scattering angles exceeding 45°. In the experiment, however, the fanning maxima are typically measured at scattering angles of about 15°–20° to the a axis, even for large pumping beam diameters. This indicates that the initial distribution of noise has finite width and is centered around the direction of propagation of the pump beam.

Figure 5 shows the calculated far-field distribution of fanning light for $L = 3$ mm and the geometry of Fig. 1. The scattering noise was assumed to have a Gaussian spectrum in Fourier space with the half-width of $\theta_n = 24°$ outside the crystal: $I_{in} \propto \exp[-2(tg^2\theta_h + tg^2\theta_v)/tg^2\theta_n]$. Figure 5 spans the same angular range as Figs. 2 and 3 with the pumping beam being in the middle of the figure. Only the beams lying to the right of the pump beam are amplified by the two-wave-mixing process and give a significant intensity on the output screen. The similarity with the experimental picture of Fig. 1 is remarkable. For signals propagating at 20° to the a axis, the calculated angle between the petals is less than 2° apart from the angle measured experimentally (55°).

In conclusion, we have explained the origin of the three petals commonly seen in the far-field fanning pattern for $BaTiO_3$ crystals. We have shown that an approach that accounts for all possible crystal deformations predicts the observed distribution of fanning light. The plane-wave approximation used in the paper is sufficient to reproduce qualitatively the experimental results. However, for a more quantitative analysis, one would need to account also for the effect of pump depletion, finite beam size, and reflections at the crystal surfaces. Evidently, the geometry presented in this paper, though very common, is not the only one possible in $BaTiO_3$. We have verified that the set of equations (1) correctly predicts the observed fanning pattern for other typical crystal orientations and pump beam polarizations. As shown above, the same is not true if a theory based on clamped or unclamped tensors is used. However, there exist some particular geometries for which both approaches give qualitatively (but not quantitatively) similar results. The present investigation confirms that the optimum geometries for photorefractive wave-mixing experiments can be calculated only when one accounts for all relevant optical, electrical, and mechanical properties of the material.

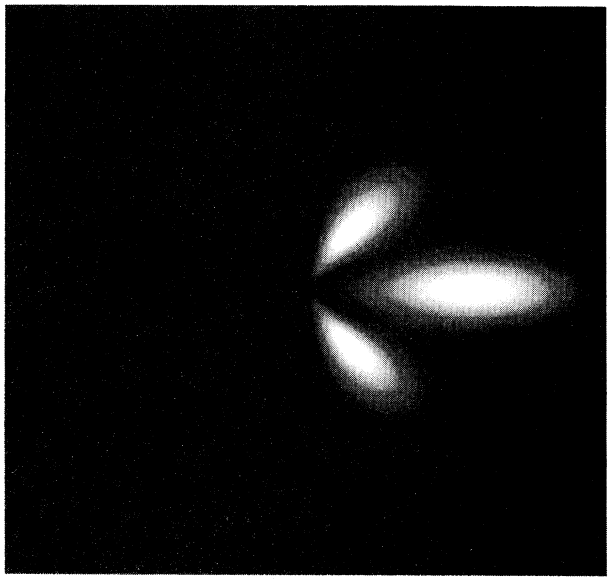

FIG. 5. A theoretical far-field intensity distribution corresponding to Fig. 1. The initial noise has a Gaussian distribution in Fourier space with the characteristic divergence of 24° outside the crystal.

This work was supported by NSF Grant No. PHY90-12244 and the Optoelectronic Computing Systems Center, a NSF Engineering Research Center. G. M. acknowledges support from the Swiss National Science Foundation.

[1] V. V. Voronov, I. R. Dorosh, Yu. S. Kuz'minov, and N. V. Tkachenko, Kvant. Electron. (Moscow) **10**, 1234 (1980). [Sov. J. Quantum Electron. **10**, 1346 (1980)].

[2] O. Yeh, *Introduction to Photorefractive Nonlinear Optics* (Wiley, New York, 1993).

[3] A. A. Izvanov, A. E. Mandel, N. D. Khatkov, and S. M. Shandarov, Avtometriya No. 2, 79 (1986) [Optoelectron. Data Process. Instrum. No. 2, 80 (1986)].

[4] S. I. Stepanov, S. M. Shandarov, and N. D. Khat'kov, Fiz. Tverd. Tela (Leningrad) **29**, 3054 (1987) [Sov. Phys. Solid State **29**, 1754 (1987)].

[5] P. Günter and M. Zgonik, Opt. Lett. **16**, 1826 (1991).

[6] P. Pauliat, M. Mathey, and G. Roosen, J. Opt. Soc. Am. B **8**, 1942 (1991).

[7] S. Shandarov, Appl. Phys. A **55**, 91 (1992).

[8] M. Zgonik, R. Schlesser, I. Biaggio, E. Voit, J. Tscherry, and P. Günter, J. Appl. Phys. **74**, 1287 (1993).

[9] N. V. Kukhtarev, V. B. Markov, S. G. Odulov, M. S. Soskin, and V. L. Vinetskii, Ferroelectrics **22**, 949 (1979).

[10] M. Zgonik, K. Nakagawa, and P. Günter, J. Opt. Soc. Am. B (to be published).

[11] M. Zgonik, P. Bernasconi, M. Duelli, R. Shlesser, P. Günter, M. H. Garrett, D. Rytz, Y. Zhy, and X. Wu, Phys. Rev. B **50**, 5941 (1994).

[12] P. Bernasconi, M. Zgonik, and P. Günter, J. Opt. Soc. Am. B (to be published).

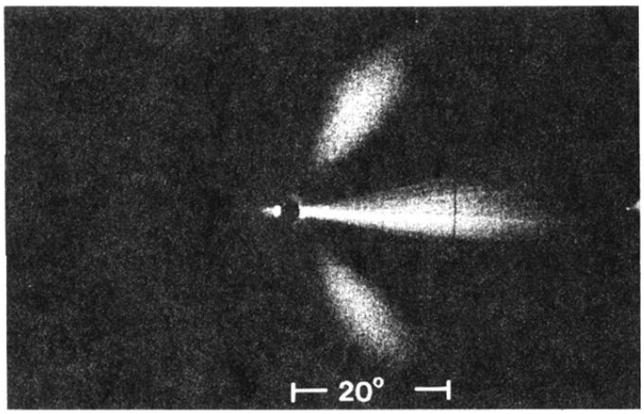

FIG. 1. Far-field intensity distribution of amplified scattered light (fanning) for a pumping beam ($\lambda = 514$ nm) propagating through a photorefractive crystal of $BaTiO_3$ along the *a* axis. Both the pump and the fanning have extraordinary polarization. The crystal *c* axis points to the right. The pump beam is blocked by the dark spot in the middle; the power going into the petals is about 10% of that of the transmitted pumping beam.

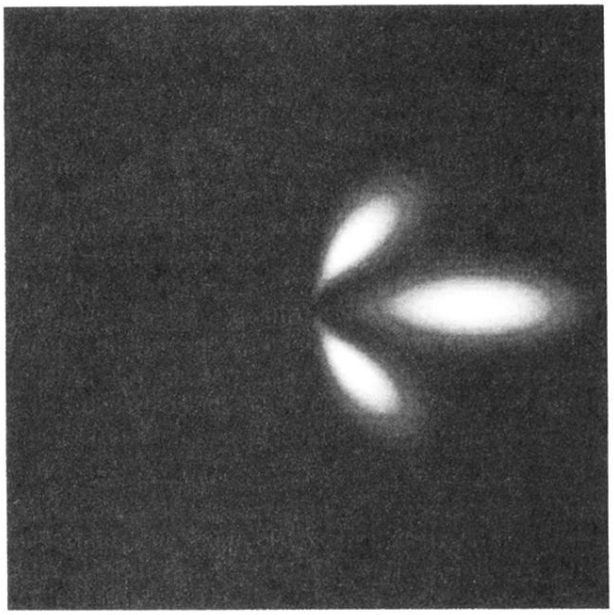

FIG. 5. A theoretical far-field intensity distribution corresponding to Fig. 1. The initial noise has a Gaussian distribution in Fourier space with the characteristic divergence of 24° outside the crystal.